ADVANCING EARTH AND SPACE SCIENCES

Geophysical Research Letters

RESEARCH LETTER
10.1029/2024GL110632

Special Collection:
Space Weather Events of 2024 May 9-15

GOLD Observations of the Merging of the Southern Crest of the Equatorial Ionization Anomaly and Aurora During the 10 and 11 May 2024 Mother's Day Super Geomagnetic Storm

Deepak Kumar Karan[1], Carlos R. Martinis[2], Robert E. Daniell[3], Richard W. Eastes[1], Wenbin Wang[4], William E. McClintock[1], Robert G. Michell[5], and Scott England[6]

[1]Laboratory for Atmospheric and Space Physics, University of Colorado, Boulder, CO, USA, [2]Astronomy Department, Center for Space Physics, Boston University, Boston, MA, USA, [3]Ionospheric Physics, Stoughton, MA, USA, [4]High Altitude Observatory, National Center for Atmospheric Research, Boulder, CO, USA, [5]Goddard Space Flight Center, Greenbelt, MD, USA, [6]Virginia Polytechnic Institute and State University, Blacksburg, VA, USA

Key Points:

- EIA crests between ~70° and 35°W moved poleward, with northern and southern crest reaching ~38°N and ~35°S Mlat in the American sector
- Southern EIA crest moved poleward with a speed of ~450 m/s near ~55°W Glon during strong IMF Bz and d (Dst)/dt
- First observation of the merging of an EIA crest with the aurora indicating no mid-latitude ionosphere

Supporting Information:

Supporting Information may be found in the online version of this article.

Correspondence to:

D. K. Karan,
Deepak.Karan@lasp.colorado.edu

Citation:

Karan, D. K., Martinis, C. R., Daniell, R. E., Eastes, R. W., Wang, W., McClintock, W. E., et al. (2024). GOLD observations of the merging of the Southern Crest of the equatorial ionization anomaly and aurora during the 10 and 11 May 2024 Mother's Day super geomagnetic storm. *Geophysical Research Letters*, *51*, e2024GL110632. https://doi.org/10.1029/2024GL110632

Received 3 JUN 2024
Accepted 25 JUL 2024

Abstract Using NASA's Global-scale Observations of the Limb and Disk (GOLD) imager, we report nightside ionospheric changes during the G5 super geomagnetic storm of 10 and 11 May 2024. Specifically, the nightside southern crest of the Equatorial Ionization Anomaly (EIA) was observed to merge with the aurora near the southern tip of South America. During the storm, the EIA southern crest was seen moving poleward as fast as 450 m/s. Furthermore, the aurora extended to mid-latitudes reaching the southern tips of Africa and South America. The poleward shift of the equatorial ionospheric structure and equatorward motion of the aurora means there was no mid-latitude ionosphere in this region. These observations offer unique insights into the ionospheric response to extreme geomagnetic disturbances, highlighting the complex interplay between solar activity and Earth's upper atmosphere.

Plain Language Summary On Earth's nightside during the super geomagnetic storm that occurred on 10 May 2024, NASA's GOLD imager saw something new: a part of Earth's ionosphere, the southern peak of what typically appears as a double-peaked structure in the ionospheric density at equatorial and low latitudes, merged with the aurora near the southern tip of South America. This has never been reported before. Additionally, the boundary of the aurora expanded further equatorward than usual. These observations of what happened in the Earth's ionosphere during this super storm are reported for the first time in this study.

1. Introduction

The terrestrial ionosphere can be divided into three latitude regions based on Earth's magnetic field topology: (a) equatorial and low-latitude ionosphere extending to ±~20° magnetic latitude (Mlat), where the magnetic field lines are closed and nearly horizontal; (b) the high-latitude polar cap and auroral ionosphere (~60° to ~90° Mlat) where magnetic field lines are open and nearly vertical; and (c) the mid-latitude ionosphere (~20° to ~60° Mlat) located between the other two (Hunsucker & Hargreaves, 2003; Schunk & Nagy, 2009).

In the equatorial and low-latitude ionosphere, Equatorial Ionization Anomaly (EIA) (also known as the Appleton Anomaly) is a persistent feature that appears as a double-peaked structure in the latitudinal distribution of the ionospheric density (Appleton, 1946; Eastes et al., 2019). Its formation is generally explained by the uplift of the plasma to higher altitudes and at latitudes in the equatorial region through E × B drifts, along with subsequent plasma motion parallel to the magnetic field B due to pressure gradient force and gravity (Heelis, 2004). Under geomagnetically quiet conditions, the EIA crests are typically near ±~10–20° Mlat depending on the solar activity (Balan et al., 2018; Eastes et al., 2023). The changes in the EIA crests latitude and brightness depend on several factors, including neutral winds, electric fields, magnetic declination, ion production and loss rates, and the subsolar point location (Eastes et al., 2023). During geomagnetic storms, the injection of energy from the solar wind and magnetosphere causes profound changes in these factors that in turn alter the EIA morphology. Previous studies showed that during a weak geomagnetic storm with SYM-H ~−60 nT in a solar minimum year, 2020, the EIA crests shifted ~8° poleward and reached ~15° Mlat (Karan, Eastes, Daniell, et al., 2023). A moderate geomagnetic storm with SYM-H ~175 nT in a solar maximum year, 2023, shifted the EIA crests poleward by ~11° and reached ~25° Mlat (Karan et al., 2024). During the 30 October 2003 Halloween storm, the EIA

expanded to ∼28° Mlat which was attributed to the combined effect of an eastward penetration electric field and wind transport (Lin et al., 2005; Mannucci et al., 2005).

Like the expansion of the EIA crests during geomagnetic storms, at high-latitudes the aurora also expands from its quiet time location (e.g., ∼70° Mlat) (Lassen et al., 1988). During extremely intense geomagnetic storms, the auroral oval can expand equatorward to ∼40°–50° Mlat (Akasofu, 1966). During the 20–25 March 1940 geomagnetic storm, auroral oval reaching ∼40° Glat was reported (Hayakawa et al., 2022).

Recently, a super geomagnetic storm, classified as G5, occurred on 10 May 2024. This geomagnetic storm is the most intense storm recorded within the past two solar cycles (O'callaghan & Billings, 2024). In this study, we report on NASA's Global-scale Observations of the Limb and Disk (GOLD) mission's nighttime observations during this storm. These observations reveal a significant poleward motion of the EIA crests, along with equatorward expansion of the aurora, which leads to the merging of the EIA crests with the aurora. This is the first time such an event has been reported and represents the disappearance of the mid-latitude ionosphere during this storm.

2. Data

The data utilized in this investigation comprises nocturnal partial disk images obtained from the GOLD instrument which is in a geostationary orbit at 47.5° W. The GOLD instrument consists of two independent channels denoted as A and B, each equipped with a scan mirror and interchangeable slits. These images of the far ultraviolet (FUV) wavelength range (∼134–162 nm) emissions from Earth. Detailed descriptions of the instrument and its observations can be found in prior works (Eastes et al., 2017, 2019, 2020; Karan et al., 2020; Karan, Eastes, Martinis, et al., 2023; McClintock et al., 2020). GOLD measures the nocturnal airglow emission at OI 135.6 nm, which originates from the recombination of atomic oxygen ions and electrons in the Earth's ionosphere. Given that the emission intensity correlates with the square of the electron density, it reaches its peak at the F layer maximum assumed to be at 300 km altitude during image geolocation. GOLD images the South American, the Atlantic, and the West African sectors, from 19 to 22 local time (LT). These images provide, with clarity, the spatio-temporal progression of various nightside ionospheric-thermospheric phenomena.

Solar wind density and speed, the interplanetary magnetic field and geomagnetic indices are used to provide context for the GOLD observations. Ionosonde observations from Cachoeira Paulista (22.7°S Glat, 45.0°W Glon, 20°S Mlat) and Bahia Blanca (38.7°S Glat, 62.3°W Glon, 27°S Mlat) are used to investigate the ionospheric changes during the storm. The in situ electron density measurements by Swarm Alpha (A) and Swarm Charlie (C) satellites at an altitude of ∼462 km (Friis-Christensen et al., 2006) are used to cross-check the EIA crest latitudes against those observed by GOLD. Optical airglow emissions from all-sky-imagers (ASIs) at the Sutherland (32.37°S Glat, 20.81°E Glon, 40.73°S Mlat) and Rio Grande (53.79°S Glat, 67.75°W Glon, 40.35°S Mlat) Observatories are also investigated to confirm the GOLD's observations.

3. Results and Discussion

Figure 1 presents 135.6 nm images captured by GOLD on the night of the storm, 10 and 11 May 2024. Images are selected to cover all the longitudes in the GOLD field of regard and to avoid repetition at similar longitudes. All the images in this night are available as Movie S1. The brightness in these images is saturated above 700 R. The images illustrate enhanced brightness patches on either side of the magnetic equator, which are the EIA crests. The equatorward sides of the red patches at higher latitudes indicate the equatorward boundary of the aurora.

With the progression of time, both EIA crests are seen to move rapidly poleward, particularly in the Atlantic and South America sectors. The southern EIA crest reaches latitudes in the southern Atlantic Ocean and near the southern tip of South America (Panels d–i). It is observed to merge repeatedly with the aurora (see 23:10 UT and 00:22 UT images in Movie S1 and Panel i in Figure 1). A study by Martinis et al. (2015) during a moderate geomagnetic storm showed the simultaneous incursion of equatorial plasma bubbles (EPBs) into mid-latitudes (∼40° Mlat) and a stable auroral red (SAR) arc, between ∼45° and 50° MLat, where the ionospheric trough was also detected by GPS TEC maps. That study stressed the reduction of the mid-latitude ionosphere to a few degrees in latitude. In the present case, instead of observing typical mid-latitude characteristics such as low-density plasma, reduced airglow and the presence of MSTIDs (Medium Scale Traveling Ionospheric Disturbances), we measured a crest of the EIA, a low latitude process, and the high-latitude aurora. Therefore, our study constitutes the first observation of the disappearance of the mid-latitude ionosphere. The southern EIA crest

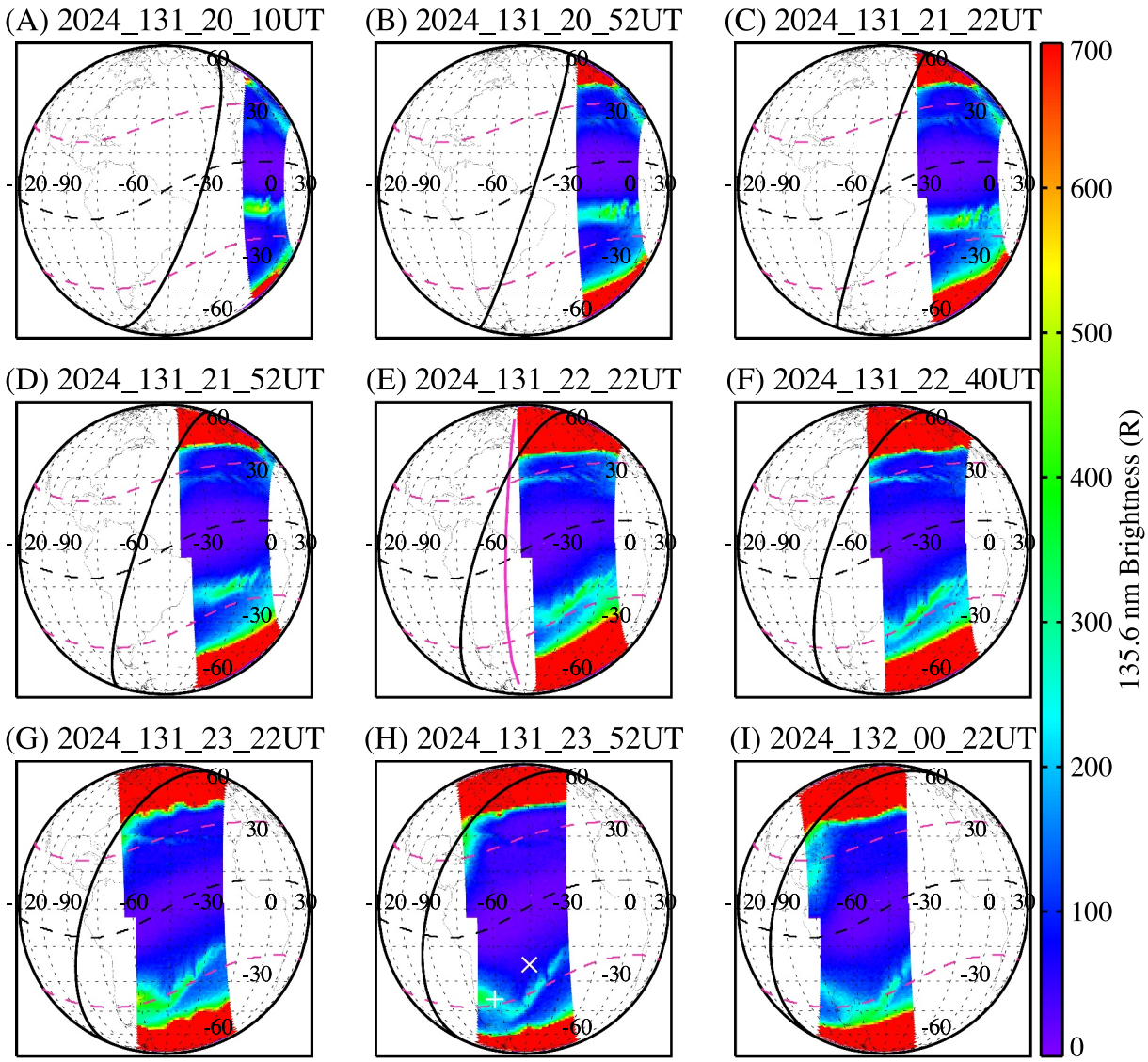

Figure 1. GOLD nighttime 135.6 nm images on 10 and 11 May 2024 (Day of the year 131 and 132). The dashed and solid black line represent the geomagnetic equator and the sunset terminator, respectively. The dashed magenta lines indicate ±30°Mlat. The solid magenta line in panel E indicates the Swarm A orbit. The white "X" and "+" symbols in panel (h) indicate the locations of the ionosonde at Cachoeira Paulista and Bahia Blanca, respectively.

appeared as a "V" shape at ~40°W Glon at 22:40 UT (Panel f; also, in Movie S1) that gradually moved to the west with time. The aurora reached ~30°S Glat over Western Africa (Panel b, c) and the Atlantic (Panels e, f). In the North and South America sector, it reached ~35°N and ~50°S Glat (Panels h–i).

Solar wind parameters for 10 and 11 May 2024 storm are shown in Figure 2, panels a (interplanetary magnetic field north-south component, IMF Bz) and b (solar wind proton density and speed). Geomagnetic conditions are shown in Panel c (Dst index with its hourly rate of change). The thick black line at the bottom of panel c marks the time of GOLD observations. The main phase of the storm started around 16:30 UT on 10 May with sudden changes (southward turning) in the IMF Bz, which reached ~−30 nT, and increases in solar wind density and speed, which reached ~700 km/s and ~30/cc, respectively. The main phase persisted until ~03:00 UT on 11 May when Dst reached a minimum value of ~−400 nT. Approximately 4 hr after the initiation of the main phase, GOLD nighttime observations began as Dst reached a value of ~−350 nT. GOLD's nightside observations, depicted in Figure 1, occurred during the main phase of the storm.

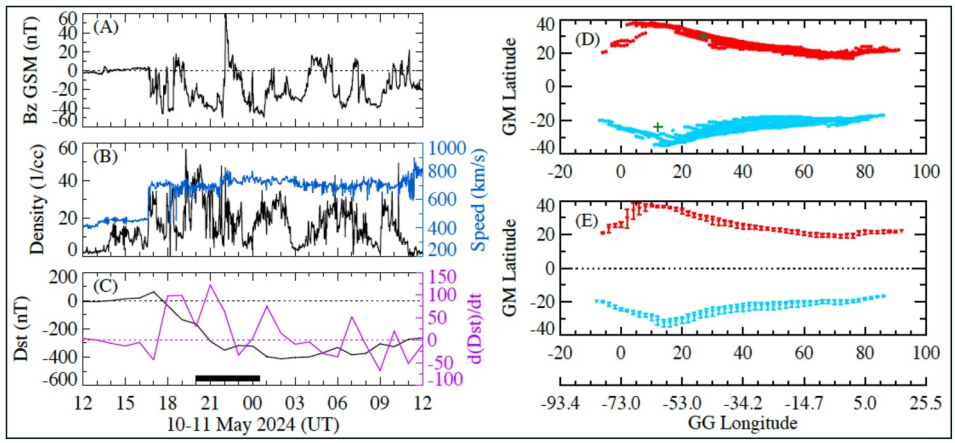

Figure 2. (left): Solar wind data and geomagnetic indices. (a) IMF Bz, (b) solar wind density and flow speed, (c) Dst and d (Dst)/dt. The thick black line at the bottom of panel C indicates the times of GOLD observations; (right) EIA crests latitudes on 10 and 11 May 2024. (d) EIA crests latitudes, North (red) and South (blue) (green) obtained from all the images on 10 and 11 May 2024. The plus symbols mark Swarm observations; (e) the average EIA crest latitudes from panel (d) and uncertainties.

We investigated the poleward motion of the EIA crest by first identifying the latitudes at which the northern and southern EIA crests peak in all images (refer to Movie S1) obtained by GOLD. These images were then transformed into quasi-dipole geomagnetic coordinates (Laundal & Richmond, 2017) using the International Geomagnetic Reference Field scalar potentials (Alken et al., 2021). This transformation enabled us to analyze variations in airglow brightness with respect to magnetic latitudes. By applying this method to all images, we determined the latitudes of the crests, as shown in Figure 2, panel d. The red and blue color dots indicate the northern and southern crest latitudes. There are multiple dots at some longitudes because crest latitudes were obtained from multiple images. We computed the average and standard deviation of both crest latitudes (Panel e) in corresponding colors.

The EIA crests were observed more poleward within the ~70°–35°W Glon range compared to the east of ~35°W. The maximum poleward location of the northern and southern EIA crests was observed between ~60°–65°W Glon (Panel d) with average crest latitudes at ~36.5°N and ~33°S Mlat, respectively (Panel e). The farthest poleward values of the northern and southern EIA crests were ~38°N and ~35°S Mlat (Panel d) which indicates a super fountain effect (Rout et al., 2019; Tsurutani et al., 2008). At this longitude region, the equatorward edge of the aurora shifted to mid-latitudes (~45°N and ~36°S Mlat), as can be seen from the equatorward edge of the red patch in Figure 1 panel i. This indicates a more equatorward incursion of the aurora in the southern hemisphere. Thus, the poleward side of the southern EIA crest (~35°S Mlat) merged with the equatorward edge of the aurora australis (~36°S Mlat). At ~10°Mlon, the 00:22 UT image (see Figure 1 Panel i and Movie S1) showed increasing brightness from the EIA, followed by the edge of the aurora moving to a higher latitude. The recurrence of these changes suggests that the EIA and aurora are influencing one another.

The southern EIA crest started to evolve into a "V" shape structure at ~40°W Glon in the 22:40 UT image (Figure 1 Panel f and Movie S1). At the location of the "V" sunset occurred around 21 UT. At that time, the storm was rapidly intensifying as IMF Bz and d(Dst)/dt reached maxima of ~ −40 nT and ~ −125 nT/hr, respectively (Figure 2 Panel A). These conditions suggest a prompt penetration of electric field into the equatorial and low latitudes at the dusk sector due to under-shielding conditions (Fejer et al., 1979; Karan, Eastes, Daniell, et al., 2023; Karan et al., 2024; Kelley et al., 2003; Martinis et al., 2005). Thus, the observed poleward expansion of the southern EIA crest and evolution into a "V" shape may be due to resulting increase the ion drifts at low latitudes.

As described above, the poleward shift of the EIA crest in the ~70°–35°W Glon range points to a strengthening of the upward drifts at the magnetic equator and low latitudes due to prompt penetration electric fields that moved the equatorial ionosphere to higher altitudes and latitudes. This can be confirmed by ionosonde measurements at these longitudes. After the sunset at ~22 UT, the peak electron density height (hmF2) measured by the ionosonde

at Cachoeira Paulista (22.7°S Glat, 45.0°W Glon, 20°S Mlat) increased from ∼300 to ∼500 km while the critical frequency of the F2 layer (foF2) decreased from ∼10 to 4 MHz. A mid-latitude ionosonde at Bahia Blanca (38.7°S Glat, 62.3°W Glon, 27°S Mlat) measured an increase in the foF2 from ∼8 to ∼17 MHz, with decrease in hmF2 at that time. The ionosonde measurements are shown in Figure S1. The ionosonde observations indicate that most of the ionosphere from the magnetic equator to ∼20°S Mlat was moved poleward which resulted in an increase in foF2 at ∼27°S Mlat. These measurements suggest the strengthening of the upward (perpendicular to B) plasma drift over these longitudes.

In addition, we investigated the poleward shift of the southern EIA crest with time. At ∼35°W Glon the southern EIA crest shifted poleward from ∼18°S Mlat at 21:10 UT to ∼27°S Malt at 22:25 UT with an inferred speed of ∼280 m/s. We also investigated the in situ electron density (Ne) measurements from Swarm A satellite for the orbit near the longitudes of maximum EIA poleward shift (∼55°W Glon). The orbit is shown in Figure 1 panel e. Swarm A crossed the geographic equator at 22:40 UT. The peak Ne latitudes are marked as green "+" symbols in Figure 2 Panel d. Swarm A measured the northern and southern EIA crests at about 30°N and 24°S Mlat at 22:35UT and 22:50 UT, respectively. When GOLD scanned the same southern longitude ∼20 min later (23:10 UT scan) the southern crest had moved ∼5° poleward and reached 29°S Mlat. This corresponds to a motion of ∼450 m/s polewards. These poleward motions of 280 and 450 m/s are many times larger than those seen during quiet times, for example, (Scherliess & Fejer, 1999). Assuming this motion is the result of E × B drift, it is possible to estimate the electric fields that were present in this region. Taking into account the inclination of the magnetic field relative to the horizontal plane and using a representative field strength of 24,000 nT estimated electric fields of ∼8 and ∼12 mV/m at ∼35 W and 55°W Glon are obtained which could have created the super fountain effect.

Figure 3 presents additional effects observed during the storm. The top panel shows two GOLD images at 21:10 UT (left) and 22:10 UT (right) where westward tilted EPBs reaching high latitudes are observed. Westward tilted EPBs piercing through the EIA crests are also observed at the West African sector. Their foot points are marked by red dots. Changes in the locations of the dots in the left and right images clearly show the westward motion of the EPBs in this latitude region. The westward motion of the EPBs at mid-latitudes tilt the EPBs westward as has been seen previously in strong storms (e.g., Karan et al., 2024). In the South American sector near 45°W Glon, EPBs reached ∼30°S Mlat (See the right wing of the "V" shaped EIA structure in GOLD image at 23:52 UT in Figure 1 and Movie S1).

The bottom panel of Figure 3 shows concurrent GOLD images of the OI 135.6 nm (left) and N_2 (Lyman-Birge-Hopfield bands, LBH) emissions (right). The 135.6 nm emissions extend over the southern tip of South America and further north than the LBH emissions. In addition to the 135.6 nm emissions energetic particles in the aurora also produce the LBH emissions, if the particles have sufficient energy to penetrate to altitudes where the N_2 concentration is significant relative to that of atomic oxygen. The occurrence of 135.6 nm emission without coincident LBH emissions indicates an area where particle energies were low, only hundreds of eV. These areas are likely where the red aurora, which is sometime seen from the ground, occurred. The red aurora (OI 630.0 nm) is typically seen equatorward of the normal green line (OI 557.7 nm) aurora, and it occurs at higher altitudes, mostly above 300 km. At these higher altitudes, there is almost no molecular nitrogen (N_2) relative to atomic oxygen. The result is emissions from atomic oxygen but very little from molecular nitrogen.

GOLD measurements are confirmed by observations from the Boston University network of ASIs, which capture airglow emissions at 630.0 and 557.7 nm. During the initial phase of the geomagnetic storm, the ASI in Sutherland, South Africa measured significant 630.0 nm airglow enhancements linked to the aurora australis. These enhancements, initially observed in the south, moved equatorward and reached zenith. Later there were similar observations over South America. Over the southern tip of South America, the ASI at the Rio Grande Observatory also detected an increased 630.0 nm emission from the aurora. Figure 4 displays a sequence of four images from Sutherland (∼20:30–22:00 UT; top panel) and Rio Grande (∼00:00–00:30 UT; bottom panel) that were unwrapped assuming an emission height of 300 km. Cloudy skies did not allow continuous observations of the auroral incursion. The two panels clearly show the equatorward expansion of auroral displays that reached an unusual low magnetic latitude, ∼40°Mlat. In both sites the activity saturated the images. These observations correlate with the GOLD's 135.6 nm images taken on 10 and 11 May (see Figure 1 Panels a–c, i), showing enhancements in 135.6 nm reaching the southern tips of Africa and South America, respectively.

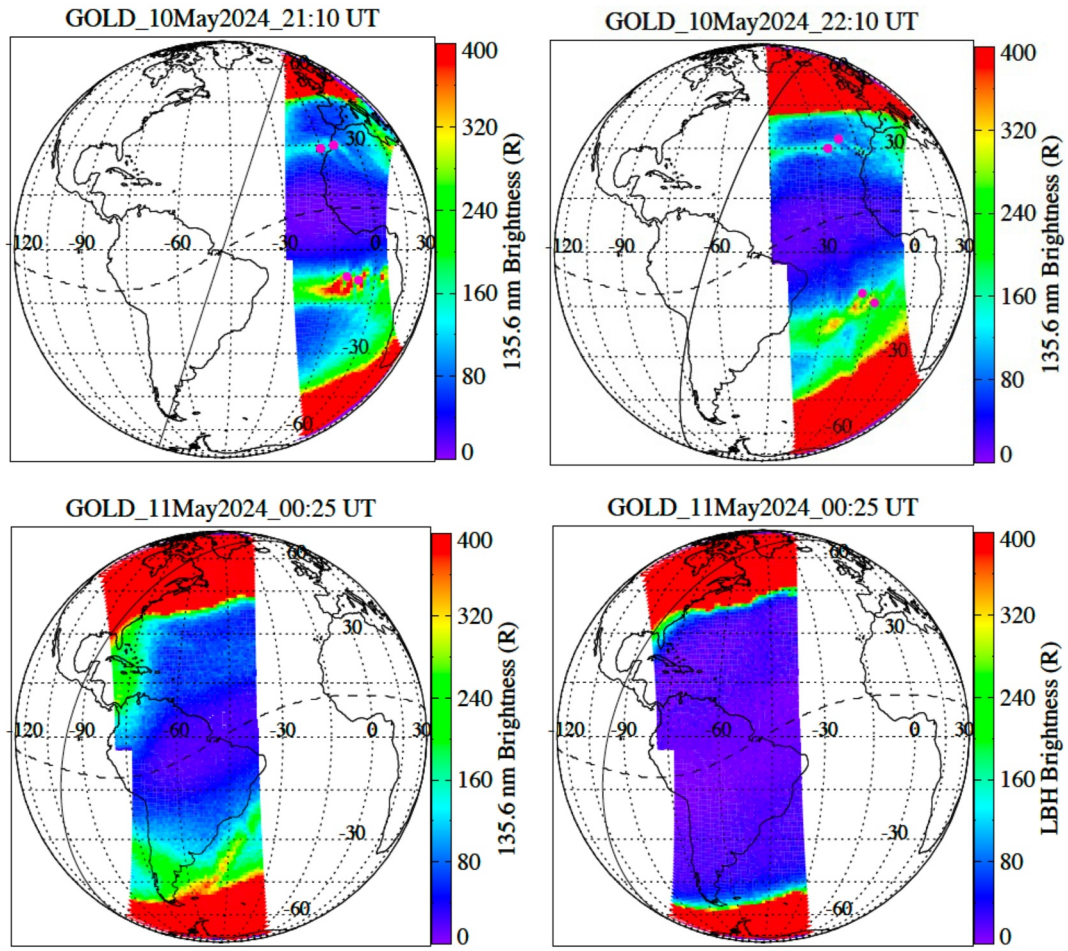

Figure 3. (top) GOLD nighttime images at 21:10 UT (left) and 22:10 UT (right). The EPB foot points are marked by red dots, clearly showing westward tilt and westward motion; (bottom) GOLD nighttime images in OI 135.6 nm (left) and LBH emission (right). The 135.6 nm images clearly reach lower latitudes than the LBH images.

4. Summary

We report on unprecedented observations of the nightside ionosphere captured by the GOLD imager during the 10 and 11 May 2024 super geomagnetic storm. Following are the key results:

i. The northern and southern EIA crests reached ~38°N and ~35°S Mlat, respectively. The southern EIA crest moved poleward with speeds of ~280 and ~450 m/s at ~ 35°W and ~55°W Glon, respectively, indicative of the rapid poleward motion that occurred over a wide range of longitudes.
ii. The southern EIA crest evolved into a "V" shape near 40°W Glon at 22:40 UT that then drifted west. At these longitudes, there was a significant poleward shift of the southern EIA crest during the period of maxima IMF Bz and d(Dst)/dt of ~−40 nT and ~ −125 nT/hr, respectively. This suggests a prompt penetration of electric field into the equatorial and low latitudes. Increased hmF2 and decreased foF2 at ~20°S Mlat from Cachoeira Paulista ionosonde and increased foF2 at ~27°S Mlat from Bahia Blanca ionosonde confirm a strengthening of the upward plasma drift.
iii. The aurora reached ~30°S Glat over the Western African and Atlantic sectors. It moved to mid-latitudes reaching ~45°N and ~36°S Mlat over the American sector. The auroral OI 135.6 nm emission reached lower latitudes than the N_2 LBH emission, in agreement with ground based all-sky imagers observations of only red line (OI 630 nm) enhancements.

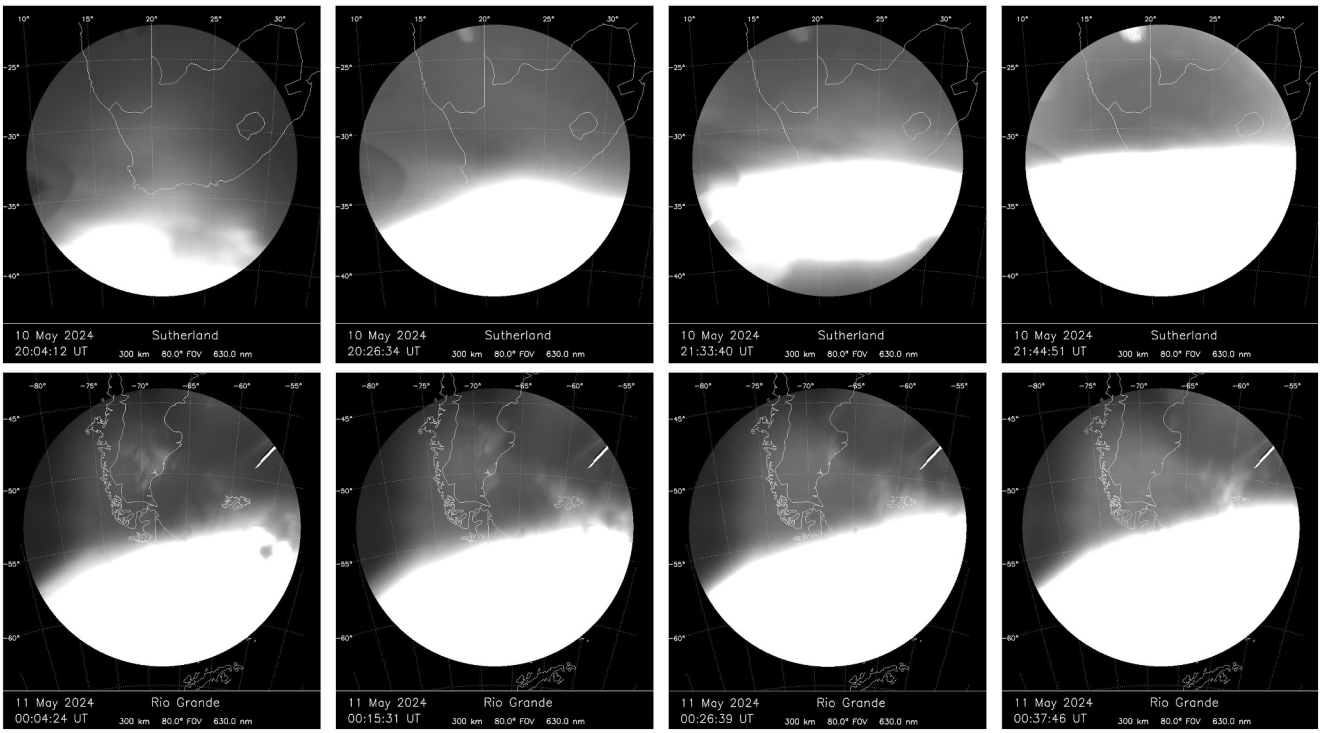

Figure 4. (top) all-sky images from Sutherland between 20:04 and 21:56 UT; (bottom) all-sky images from Rio Grande between 00:04 and 00:37 UT. Equatorward expansion of enhancements in 630.0 nm airglow is observed at both locations. Images are unwrapped at 300 km with zenith angles less than 80°.

iv. The poleward shift of the equatorial ionospheric structure, equatorward motion of the aurora, and the merging of these two structures seen by GOLD means there was no mid-latitude ionosphere. They merge multiple times and when they do the resulting changes in the EIA and aurora suggests that the merging affects each of them. This is the first reported observation of the nighttime EIA crest merging with the aurora.

Data Availability Statement

The GOLD data are available from the GOLD Science Data Center (https://gold.cs.ucf.edu/data/search/). The solar wind parameters are obtained from SWPC data service center (https://services.swpc.noaa.gov/products/solar-wind/). The geomagnetic indices are obtained from https://www.gfz-potsdam.de/en/hpo-index and https://isgi.unistra.fr/data_download.php. Bahia Blanca ionosonde data can be found at http://www.eswua.ingv.it/. Cachoeira Paulista ionosonde data are obtained using the SAO Explorer software from the Global Ionospheric Radio Observatory website (https://ulcar.uml.edu/SAO-X/SAO-X.html and http://spase.info/SMWG/Observatory/GIRO). Swarm in situ Ne data were obtained from (https://swarm-diss.eo.esa.int/#swarm/Level1b/Entire_mission_data/EFIx_LP). Quick look all-sky images and movies from Sutherland and Rio Grande can be obtained from www.buimaging.com. The ionosonde data from Bahia Blanca station are obtained from the Upper atmosphere physics and radiopropagation Working Group (Marcocci et al., 2020).

Acknowledgments
This research was supported by NASA contract 80GSFC18C0061 to the University of Colorado. CM acknowledges the support of NSF Aeronomy Grant 2152365. CM thanks the Director and personnel of SANSA (South African National Space Agency) for supporting the Sutherland all-sky imager. CM thanks the Director of EARG (Estacion Astronomica Rio Grande) and Jose Luis Hormaechea for their continuing support of the Rio Grande ASI. The National Center for Atmospheric Research is Sponsored by the National Science Foundation. WW is also supported in part by the NASA award 80NSSC22M0163 and Grant 80NSSC20K0356.

References

Akasofu, S.-I. (1966). The auroral oval, the auroral substorm, and their relations with the internal structure of the magnetosphere. *Planetary and Space Science*, *14*(7), 587–595. https://doi.org/10.1016/0032-0633(66)90043-2

Alken, P., Thébault, E., Beggan, C. D., Amit, H., Aubert, J., Baerenzung, J., et al. (2021). International geomagnetic reference field: The thirteenth generation. *Earth Planets and Space*, *73*(1), 49. https://doi.org/10.1186/s40623-020-01288-x

Appleton, E. V. (1946). Two anomalies in the ionosphere. *Nature*, *157*(3995), 691. https://doi.org/10.1038/157691a0

Balan, N., Liu, L. B., & Le, H. J. (2018). A brief review of equatorial ionization anomaly and ionospheric irregularities. *Earth and Planetary Physics*, *2*(4), 1–19. https://doi.org/10.26464/epp2018025

Eastes, R. W., Karan, D. K., Martinis, C., Daniell, R. E., Gan, Q., Burns, A. G., & McClintock, W. E. (2023). GOLD observations of longitudinal variations in the nighttime equatorial ionization anomaly (EIA) crests' latitudes. *Journal of Geophysical Research: Space Physics*, *128*(4), e2022JA031007. https://doi.org/10.1029/2022JA031007

Eastes, R. W., McClintock, W. E., Burns, A. G., Anderson, D. N., Andersson, L., Aryal, S., et al. (2020). Initial observations by the GOLD mission. *Journal of Geophysical Research: Space Physics*, *125*(7), e2020JA027823. https://doi.org/10.1029/2020JA027823

Eastes, R. W., McClintock, W. E., Burns, A. G., Anderson, D. N., Andersson, L., Codrescu, M., et al. (2017). The global-scale observations of the limb and disk (GOLD) mission. *Space Science Reviews*, *212*(1–2), 383–408. https://doi.org/10.1007/s11214-017-0392-2

Eastes, R. W., Solomon, S. C., Daniell, R. E., Anderson, D. N., Burns, A. G., England, S. L., et al. (2019). Global-scale observations of the equatorial ionization anomaly. *Geophysical Research Letters*, *46*(16), 9318–9326. https://doi.org/10.1029/2019GL084199

Fejer, B. G., Gonzales, C. A., Farley, D. T., Kelley, M. C., & Woodman, R. F. (1979). Equatorial electric fields during magnetically disturbed conditions—1. The effect of the interplanetary magnetic field. *Journal of Geophysical Research*, *84*(A10), 5797–5802. https://doi.org/10.1029/JA084iA10p05797

Friis-Christensen, E., Lühr, H., & Hulot, G. (2006). Swarm: A constellation to study the Earth's magnetic field. *Earth Planets and Space*, *58*(4), 351–358. https://doi.org/10.1186/bf03351933

Hayakawa, H., Oliveira, D. M., Shea, M. A., Smart, D. F., Blake, S. P., Hattori, K., et al. (2022). The extreme solar and geomagnetic storms on 1940 March 20–25. *Monthly Notices of the Royal Astronomical Society*, *517*(2), 1709–1723. https://doi.org/10.1093/mnras/stab3615

Heelis, R. A. (2004). Electrodynamics in the low and middle latitude ionosphere: A tutorial. *Journal of Atmospheric and Solar-Terrestrial Physics*, *66*(10), 825–838. https://doi.org/10.1016/j.jastp.2004.01.034

Hunsucker, R. D., & Hargreaves, J. K. (2003). *The high latitude ionosphere and its effects on radio propagation*. Cambridge University Press.

Karan, D. K., Daniell, R. E., England, S. L., Martinis, C. R., Eastes, R. W., Burns, A. G., & McClintock, W. E. (2020). First zonal drift velocity measurement of equatorial plasma bubbles (EPBs) from a geostationary orbit using GOLD data. *Journal of Geophysical Research: Space Physics*, *125*(9), e2020JA028173. https://doi.org/10.1029/2020JA028173

Karan, D. K., Eastes, R. W., Daniell, R. E., Martinis, C. R., & McClintock, W. E. (2023). GOLD mission's observation about the geomagnetic storm effects on the nighttime equatorial ionization anomaly (EIA) and equatorial plasma bubbles (EPB) during a solar minimum equinox. *Space Weather*, *21*(3). https://doi.org/10.1029/2022SW003321

Karan, D. K., Eastes, R. W., Martinis, C. R., Daniell, R. E., Solomon, S. C., & McClintock, W. E. (2023). Unique combinations of differently shaped equatorial plasma bubbles occurring within a small longitude range. *Journal of Geophysical Research: Space Physics*, *128*(11), e2023JA031625. https://doi.org/10.1029/2023JA031625

Karan, D. K., Martinis, C. R., Eastes, R. W., Daniell, R. E., McClintock, W. E., & Huang, C. (2024). GOLD observations of equatorial plasma bubbles reaching mid-latitudes during the 23 April 2023 geomagnetic storm. *Space Weather*, *22*(6). https://doi.org/10.1029/2023SW003847

Kelley, M. C., Makela, J. J., Chau, J. L., & Nicolls, M. J. (2003). Penetration of the solar wind electric field into the magnetosphere/ionosphere system. *Geophysical Research Letters*, *30*(4). https://doi.org/10.1029/2002GL016321

Lassen, K., Danielsen, C., & Meng, C. I. (1988). Quiet-time average auroral configuration. *Planetary and Space Science*, *36*(8), 791–799. https://doi.org/10.1016/0032-0633(88)90085-2

Laundal, K. M., & Richmond, A. D. (2017). Magnetic coordinate systems. *Space Science Reviews*, *206*(1–4), 27–59. https://doi.org/10.1007/s11214-016-0275-y

Lin, C. H., Richmond, A. D., Heelis, R. A., Bailey, G. J., Lu, G., Liu, J. Y., et al. (2005). Theoretical study of the low- and midlatitude ionospheric electron density enhancement during the October 2003 superstorm: Relative importance of the neutral wind and the electric field. *Journal of Geophysical Research*, *110*(A12), A12312. https://doi.org/10.1029/2005JA011304

Mannucci, A. J., Tsurutani, B. T., Iijima, B. A., Komjathy, A., Saito, A., Gonzalez, W. D., et al. (2005). Dayside global ionospheric response to the major interplanetary events of October 29–30, 2003 "Halloween Storms". *Geophysical Research Letters*, *32*(12), 1–4. https://doi.org/10.1029/2004GL021467

Marcocci, C., Pezzopane, M., Pica, E., Romano, V., Sabbagh, D., Scotto, C., & Zuccheretti, E. (2020). *Electronic Space weather upper atmosphere database (eSWua)—HF data, version 1.0*. Istituto Nazionale di Geofisica e Vulcanologia (INGV). https://doi.org/10.13127/ESWUA/HF

Martinis, C. R., Baumgardner, J., Mendillo, M., Wroten, J., Coster, A., & Paxton, L. (2015). The night when the auroral and equatorial ionospheres converged. *Journal of Geophysical Research: Space Physics*, *120*(9), 8085–8095. https://doi.org/10.1002/2015JA021555

Martinis, C. R., Mendillo, M. J., & Aarons, J. (2005). Toward a synthesis of equatorial spread F onset and suppression during geomagnetic storms. *Journal of Geophysical Research*, *110*(A7), A07306. https://doi.org/10.1029/2003JA010362

McClintock, W. E., Eastes, R. W., Beland, S., Bryant, K. B., Burns, A. G., Correira, J., et al. (2020). Global-scale observations of the Limb and disk mission implementation: 2. Observations, data pipeline, and level 1 data products. *Journal of Geophysical Research: Space Physics*, *125*(5), e2020JA027809. https://doi.org/10.1029/2020JA027809

O'callaghan, J., & Billings, L. (2024). The strongest solar storm in 20 years did little damage, but worse space weather is coming. *Scientific American*. Retrieved from https://www.scientificamerican.com/article/the-strongest-solar-storm-in-20-years-did-little-damage-but-worse-space/

Rout, D., Pandey, K., Chakrabarty, D., Sekar, R., & Lu, X. (2019). Significant electric field perturbations in low latitude ionosphere due to the passage of two consecutive ICMEs during 6–8 September 2017. *Journal of Geophysical Research: Space Physics*, *124*(11), 9494–9510. https://doi.org/10.1029/2019JA027133

Scherliess, L., & Fejer, B. G. (1999). Radar and satellite global equatorial F region vertical drift model. *Journal of Geophysical Research*, *104*(A4), 6829–6842. https://doi.org/10.1029/1999ja900025

Schunk, R. W., & Nagy, A. (2009). *Ionospheres: Physics, plasma physics, and chemistry*. Cambridge University Press.

Tsurutani, B. T., Verkhoglyadova, O. P., Mannucci, A. J., Saito, A., Araki, T., Yumoto, K., et al. (2008). Prompt penetration electric fields (PPEFs) and their ionospheric effects during the great magnetic storm of 30–31 October 2003. *Journal of Geophysical Research*, *113*(5), A05311. https://doi.org/10.1029/2007JA012879